National Conference with International Participation

ENGINEERING MECHANICS 2008

Svratka, Czech Republic, May 12 – 15, 2008

FETI-BASED HOMOGENIZATION OF FIBROUS COMPOSITES WITH INTERFACIAL DEBONDING

P. Gruber*, J. Zeman**

Summary: *In this contribution, we present an efficient FETI-based algorithm for homogenization of fibrous composite materials with imperfect interfaces. The proposed formulation allows for a seamless combination of the initially-rigid connection, monotone traction-separation relations due to Kruis and Bittnar (2008) and contact conditions (Dostál et al., 2007). The performance of the developed algorithm is illustrated on two representative numerical examples.*

1 Introduction

Failure in fiber-reinforced composites is often initiated at the fiber-matrix interface and hence initial as well as load-induced debonding phenomena are of crucial importance when assessing overall behavior of composites, cf. (Cox and Yang, 2006). The numerical modeling of interfacial behavior within the framework of displacement-based (primal) Finite Element method is usually based on introduction of interfacial elements allowing for the appearance of a strong displacement discontinuity on the surface separating a fiber from a matrix, see e.g (Li and Ghosh, 2004; Matouš et al., 2007) and references therein. Specific material behavior is accounted for by using an appropriate traction-separation law, relating the displacement jump to the interfacial tractions via an (possibly non-linear) interfacial stiffness. When describing the perfect bonding between phases, however, the theoretically infinite interfacial stiffness leads to an ill-conditioned FEM problem resulting in critical numerics-induced stress oscillations, see e.g. (Areias and Rabczuk, 2008) for an excellent recent survey on this topic. To overcome this intrinsic problem, in the current paper we investigate an applicability of duality-based solvers to the homogenization of composites with imperfect interfacial bonding.

The rest of the paper is organized as follows. A brief overview of the first-order periodic homogenization is presented in Section 2. In Section 3, we discuss the numerical resolution of the unit cell problem using the Finite Element Tearing and Interconnecting (FETI) method (Farhat and Roux, 1991). Exploiting advances in duality-based solvers due to Dostál et al. (2007) and Kruis and Bittnar (2008), the algorithm is extended to account for a possible contact between fibers and matrix as well as limited interfacial strength. Finally, performance of the algorithm is illustrated in Section 4 on two representative examples.

Throughout the text, the standard matrix formulation of the Finite Element method, e.g. (Bittnar and Šejnoha, 1996), combined with the Voigt representation of symmetric second- and fourth-order tensors, cf. (Wikipedia, 2007), is systematically employed.

*Ing. Pavel Gruber: Department of Mechanics, Faculty of Civil Engineering, Czech Technical University in Prague, Thákurova 7, 166 29 Prague 6; tel.: +420 224 354 472; e-mail: pavel.gruber@centrum.cz

**Ing. Jan Zeman, Ph.D.: Department of Mechanics, Faculty of Civil Engineering, Czech Technical University in Prague, Thákurova 7, 166 29 Prague 6; tel.: +420 224 354 482; e-mail: zemanj@cml.fsv.cvut

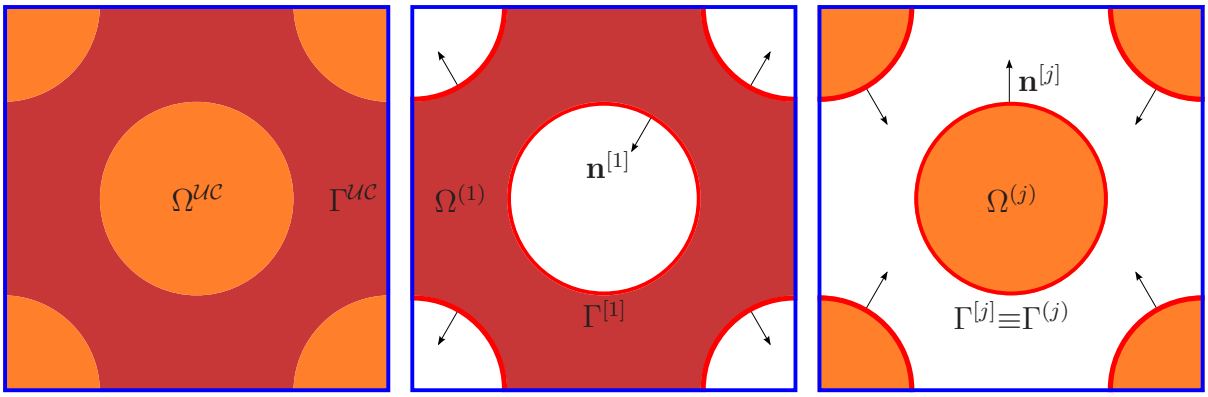

(a) Unit Cell (b) matrix (c) inclusions (fibers)

Figure 1: Decomposition of PUC.

2 Overview of periodic homogenization

In the current Section, we briefly overview essentials of the homogenization theory. Additional details can be found in, e.g., in (Michel et al., 1999; Somolová, 2007; Gruber, 2007).

2.1 Unit Cell

Consider a Periodic Unit Cell (PUC) of a composite material with long fibers, see Figure 1a. Within the PUC, we distinguish n disjoint sub-domains $\Omega^{(i)}$ with associated boundaries $\Gamma^{(i)}$. In the following text, $i = 1$ is reserved for the matrix phases, whereas $i = 2, 3, \ldots, n$ corresponds to the heterogeneities (fibers) appearing in the PUC. Therefore, it holds

$$\Omega^{\mathcal{UC}} := \bigcup_{i=1}^{n} \Omega^{(i)}, \tag{1}$$

and the following identities are valid:

$$\Omega^{(r)} \cap \Omega^{(s)} = \emptyset, \quad \text{for} \quad r \neq s, \quad \text{where} \quad r = 1, 2, ..., n \quad \text{and} \quad s = 1, 2, ..., n, \tag{2}$$

$$\overline{\Omega}^{(r)} \cap \overline{\Omega}^{(s)} = \emptyset, \quad \text{for} \quad r \neq s, \quad \text{where} \quad r = 2, 3, ..., n \quad \text{and} \quad s = 2, 3, ..., n. \tag{3}$$

It is also useful to introduce internal interfaces (denoted by square brackets instead of round ones):

$$\Gamma^{[j]} := \overline{\Omega}^{(1)} \cap \overline{\Omega}^{(j)}, \quad \Gamma^{[1]} := \bigcup_{j=2}^{n} \Gamma^{[j]}. \tag{4}$$

i.e. the boundary $\Gamma^{[j]}$ (a part of $\Gamma^{(j)}$) correspond to the interface between j-th fiber and the matrix phase, while $\Gamma^{[1]}$ is reserved for the matrix interface, cf. Figure 1b, Figure 1c. Note that in order to unify the notation, index i is assumed to range from 1 to n, while $j \in \{2, 3, \ldots, n\}$.

2.2 Fields on PUC

Let a vector $\mathbf{y}$ define the position of a point on the micro-scale (i.e. on the closure of the domain $\overline{\Omega}^{\mathcal{UC}}$). The general field $f(\mathbf{y})$ (a scalar, a vectorial or a tensorial one), the spatial average of the

function $\langle f \rangle$ and its fluctuating component f^* are defined as

$$\langle f(\mathbf{y}) \rangle := \frac{1}{|\Omega^{\mathcal{UC}}|} \int_{\Omega^{\mathcal{UC}}} f(\mathbf{y}) \, \mathrm{d}\Omega, \qquad f^*(\mathbf{y}) := f(\mathbf{y}) - \langle f(\mathbf{y}) \rangle, \quad \forall \mathbf{y} \in \Omega^{\mathcal{UC}}.$$

Moreover, it will be useful in the sequel to introduce a domain-wise decomposition of a general function f in the form:

$$f(\mathbf{y}) = \begin{cases} f^{(1)}(\mathbf{y}), & \forall \mathbf{y} \in \Omega^{(1)} \\ f^{(2)}(\mathbf{y}), & \forall \mathbf{y} \in \Omega^{(2)} \\ \quad \vdots & \\ f^{(n)}(\mathbf{y}), & \forall \mathbf{y} \in \Omega^{(n)} \end{cases}. \tag{5}$$

In addition, fields defined on $\Gamma^{[i]}$ will be denoted as $g^{[i]}$.[1] Finally, we introduce normal vectors $\mathbf{n}^{[i]}(\mathbf{y})$ to interfaces $\Gamma^{[i]}$. It holds, cf. Figure 1b and Figure 1c:

$$\mathbf{n}^{[1]}(\mathbf{y}) = -\mathbf{n}^{[j]}(\mathbf{y}), \quad \forall \mathbf{y} \in \Gamma^{[j]}. \tag{6}$$

An outer normal to the set $\Omega^{\mathcal{UC}}$, which is defined on the whole boundary $\Gamma^{\mathcal{UC}}$, is denoted as $\mathbf{n}^{\mathcal{UC}}(\mathbf{y})$.

2.3 Strain approach to homogenization

In the sequel, the *strain controlled* approach to the computational homogenization is adopted, see (Michel et al., 1999). Therefore, the PUC is subject to the loading by a *macroscopic* strain $\mathbf{E}$, which, when combined with the governing equations of continuum mechanics, yields leads to a distribution of *microscopic* displacements, strains and stresses within the PUC. The average value of the stress then yields the value of macroscopic stress $\mathbf{\Sigma}$, defining the *homogenized* constitutive equation.

2.4 Boundary conditions

Following the standard procedure of the first-order homogenization, we assume the following decomposition of the displacement field

$$\mathbf{u}^{(i)}(\mathbf{y}) = \mathbf{u}^{\mathrm{hom}} + \mathbf{u}^{*(i)}(\mathbf{y}), \tag{7}$$

where (in the tensorial notation) $\mathbf{u}^{\mathrm{hom}} = \mathbf{E} \cdot \mathbf{y}$ corresponds to an affine field due to $\mathbf{E}$, whereas the second part arises due to heterogeneity of the PUC. The corresponding strains can we written in the form

$$\boldsymbol{\epsilon}^{(i)}(\mathbf{y}) = \mathbf{E} + \boldsymbol{\epsilon}^{*(i)}(\mathbf{y}), \tag{8}$$

The macro-micro strain compatibility requires the validity of the following identity (Michel et al., 1999):

$$\oint_{\Gamma^{\mathcal{UC}}} \mathbf{u}^*(\mathbf{y})|_{\Gamma^{\mathcal{UC}}} \otimes \mathbf{n}^{\mathcal{UC}}(\mathbf{y}) \, \mathrm{d}\Gamma = \mathbf{0} \tag{9}$$

[1] Therefore the values $f^{[i]}(\mathbf{y})$ may be considered as traces of a field $f^{(i)}(\mathbf{y})$ on the interface $\Gamma^{[i]}$, cf. (Rektorys, 2007).

which corresponds to generalized kinematic boundary conditions posed on the fluctuating displacement field $\mathbf{u}^{*}(\mathbf{y})$.[2]

Next, we need to satisfy the energetic consistency condition in the form of the Hill lemma

$$\begin{aligned} \boldsymbol{\Sigma}^{\mathrm{T}}\mathbf{E} &= \langle \boldsymbol{\sigma}(\mathbf{y})^{\mathrm{T}}\boldsymbol{\epsilon}(\mathbf{y})\rangle \qquad (11)\\ &\Updownarrow \\ \langle \boldsymbol{\sigma}(\mathbf{y})^{\mathrm{T}}\boldsymbol{\epsilon}^{*}(\mathbf{y})\rangle &= \frac{1}{|\Omega^{\mathcal{UC}}|}\oint_{\Gamma^{\mathcal{UC}}}\mathbf{p}(\mathbf{y})^{\mathrm{T}}\mathbf{u}^{*}(\mathbf{y})|_{\Gamma^{\mathcal{UC}}}\,\mathrm{d}\Gamma = 0, \qquad (12)\end{aligned}$$

where $\mathbf{p}(\mathbf{y})$ denotes surface tractions on the boundary $\Gamma^{\mathcal{UC}}$.

It can be shown that the strain and the energetic consistency conditions can be satisfied when adopting a convenient choice of the kinematic or the static boundary conditions. In our case, the periodic kinematic and the anti-periodic static boundary conditions are employed to that purpose. Then, for any vectors $\mathbf{y}^{\#1}$ and $\mathbf{y}^{\#2}$ lying on two congruent boundaries, we have:

$$\mathbf{u}^{*}\left(\mathbf{y}^{\#1}\right) = \mathbf{u}^{*}\left(\mathbf{y}^{\#2}\right) \quad \wedge \quad \mathbf{p}\left(\mathbf{y}^{\#1}\right) = -\mathbf{p}\left(\mathbf{y}^{\#2}\right) \quad \wedge \quad \mathbf{n}^{\mathcal{UC}}\left(\mathbf{y}^{\#1}\right) = -\mathbf{n}^{\mathcal{UC}}\left(\mathbf{y}^{\#2}\right). \quad (13)$$

3 FETI-based solution of unit cell problem

For a numerical solution of the local problem of the homogenization, we use the FETI method which is effective even in the case of the imperfect bonding of constituents. Following the original treatment (Farhat and Roux, 1991), FETI is based on the modified Lagrange principle where surface tractions $\boldsymbol{\lambda}^{[j]}(\mathbf{y})$ (defined on the interfaces $\Gamma^{[j]}$ with orientation identical to the outer normal $\mathbf{n}^{[j]}(\mathbf{y})$) enforce the inter-domain displacement continuity. It follows from the equilibrium equation on the interface that the surface tractions $\boldsymbol{\lambda}^{[i]}(\mathbf{y})$ has to verify relations analogous to (6):

$$\boldsymbol{\lambda}^{[1]}(\mathbf{y}) = -\boldsymbol{\lambda}^{[j]}(\mathbf{y}), \quad \forall \mathbf{y} \in \Gamma^{[j]}. \qquad (14)$$

3.1 Energy functional

The energy functional $\Pi(\hat{\mathbf{u}}(\mathbf{y}), \hat{\boldsymbol{\lambda}}^{[1]}(\mathbf{y}))$ for homogeneous linear elastic constituents, which are characterized by a phase-wise constant material stiffness matrix $\mathbf{L}^{(i)}$, can be expressed as:

$$\begin{aligned} \Pi(\hat{\mathbf{u}}(\mathbf{y}), \hat{\boldsymbol{\lambda}}^{[1]}(\mathbf{y})) &= \frac{1}{2}\sum_{i=1}^{n}\int_{\Omega^{(i)}}\hat{\boldsymbol{\epsilon}}^{(i)}(\mathbf{y})^{\mathrm{T}}\mathbf{L}^{(i)}(\mathbf{y})\hat{\boldsymbol{\epsilon}}^{(i)}(\mathbf{y})\,\mathrm{d}\Omega \\ &+ \sum_{j=2}^{n}\int_{\Gamma^{[j]}}\hat{\boldsymbol{\lambda}}^{[1]}(\mathbf{y})^{\mathrm{T}}\left(\hat{\mathbf{u}}^{[j]}(\mathbf{y}) - \hat{\mathbf{u}}^{[1]}(\mathbf{y})\right)\mathrm{d}\Gamma, \qquad (15)\end{aligned}$$

[2] The operation $\mathbf{a}(\mathbf{y}) \otimes \mathbf{b}(\mathbf{y})$ appearing in Equation (9) is related to an outer product defined for two vectors $\mathbf{a}(\mathbf{y})$ and $\mathbf{b}(\mathbf{y})$ as follows:

$$\mathbf{a}(\mathbf{y}) \otimes \mathbf{b}(\mathbf{y}) := \frac{1}{2}\left(\mathbf{a}(\mathbf{y})\,\mathbf{b}(\mathbf{y})^{\mathrm{T}} + \mathbf{b}(\mathbf{y})\,\mathbf{a}^{\mathrm{T}}(\mathbf{y})\right). \qquad (10)$$

where a function $\hat{f}(\mathbf{y})$ denote a test function corresponding to a function $f(\mathbf{y})$. The functional Π is defined on a set $\mathcal{D}_\Pi$:

$$\begin{aligned}\mathcal{D}_\Pi &= \big\{\mathbf{u}(\mathbf{y}) = \mathbf{E}\mathbf{y} + \mathbf{u}^*(\mathbf{y}), \quad \forall \mathbf{y} \in \Omega^{\mathcal{UC}};\\ &\quad \mathbf{u}^*(\mathbf{y}) = \mathbf{0}, \quad \forall \mathbf{y} \in \Gamma_D^{\mathcal{UC}}; \quad \mathbf{u}^*(\mathbf{y}) \text{ periodic}, \quad \forall \mathbf{y} \in \Gamma^{\mathcal{UC}}\big\}\\ &\times \Big\{0 \le \boldsymbol{\lambda}^{[1]}(\mathbf{y})\mathbf{n}^{[1]}(\mathbf{y}) \le \lambda^{[1]}_{n,\max}(\mathbf{y}), \quad \forall \mathbf{y} \in \Gamma^{[1]};\\ &\quad -\lambda^{[1]}_{t,\max}(\mathbf{y}) \le \boldsymbol{\lambda}^{[1]}(\mathbf{y})\mathbf{t}^{[1]}(\mathbf{y}) \le \lambda^{[1]}_{t,\max}(\mathbf{y}), \quad \forall \mathbf{y} \in \Gamma^{[1]}\Big\}, \end{aligned} \tag{16}$$

where $\lambda^{[i]}_{n,\max}(\mathbf{y})$ and $\lambda^{[i]}_{t,\max}(\mathbf{y})$ correspond to an initial normal and tangential strength of i-th interface, respectively and $\mathbf{t}^{[i]}(\mathbf{y})$ denotes a tangent to the interface $\Gamma^{[i]}$ with clockwise orientation with respect to the normal vector $\mathbf{n}^{[i]}(\mathbf{y})$. Finally, $\Gamma_D^{\mathcal{UC}}$ is a part of the boundary $\Gamma^{\mathcal{UC}}$ (usually the corners of a rectangular PUC), where the Dirichlet boundary conditions are imposed, since the periodic boundary conditions prevent only the rigid body rotation of the PUC.

By splitting the microscopic fields $\boldsymbol{\epsilon}(\mathbf{y})$ and $\mathbf{u}(\mathbf{y})$ into the macroscopic and the fluctuating constituents, and disregarding the constant terms appearing in Π, we obtain a new functional

$$\begin{aligned}\Theta(\hat{\mathbf{u}}^*(\mathbf{y}), \hat{\boldsymbol{\lambda}}^{[1]}(\mathbf{y})) &= \frac{1}{2}\sum_{i=1}^{n}\int_{\Omega^{(i)}} 2\mathbf{E}^{\mathrm{T}}\mathbf{L}^{(i)}(\mathbf{y})\hat{\boldsymbol{\epsilon}}^{*(i)}(\mathbf{y}) + \hat{\boldsymbol{\epsilon}}^{*(i)}(\mathbf{y})^{\mathrm{T}}\mathbf{L}^{(i)}(\mathbf{y})\hat{\boldsymbol{\epsilon}}^{*(i)}(\mathbf{y})\,\mathrm{d}\Omega\\ &+ \sum_{j=2}^{n}\int_{\Gamma^{[j]}} \hat{\boldsymbol{\lambda}}^{[1]}(\mathbf{y})^{\mathrm{T}}\left(\hat{\mathbf{u}}^{*[j]}(\mathbf{y}) - \hat{\mathbf{u}}^{*[1]}(\mathbf{y})\right)\mathrm{d}\Gamma \end{aligned} \tag{17}$$

now defined on a set

$$\begin{aligned}\mathcal{D}_\Theta &= \big\{\mathbf{u}^*(\mathbf{y}) = \mathbf{0}, \quad \forall \mathbf{y} \in \Gamma_D^{\mathcal{UC}}; \quad \mathbf{u}^*(\mathbf{y}) \text{ periodic}, \quad \forall \mathbf{y} \in \Gamma^{\mathcal{UC}}\big\}\\ &\times \Big\{0 \le \boldsymbol{\lambda}^{[1]}(\mathbf{y})\mathbf{n}^{[1]}(\mathbf{y}) \le \lambda^{[1]}_{n,\max}(\mathbf{y}), \quad \forall \mathbf{y} \in \Gamma^{[1]};\\ &\quad -\lambda^{[1]}_{t,\max}(\mathbf{y}) \le \boldsymbol{\lambda}^{[1]}(\mathbf{y})\mathbf{t}^{[1]}(\mathbf{y}) \le \lambda^{[1]}_{t,\max}(\mathbf{y}), \quad \forall \mathbf{y} \in \Gamma^{[1]}\Big\}. \end{aligned} \tag{18}$$

3.2 Approximation

Following the basic idea of the FETI-based discretization, we approximate the field of fluctuating displacements $\mathbf{u}^*(\mathbf{y})$ independently on individual domains $\Omega^{(i)}$ with the aid of basis functions organized into a matrix $\mathbf{N}_u^{(i)}(\mathbf{y})$ and coefficients of the linear combination organized into a vector $\mathbf{d}_u^{(i)}$:

$$\mathbf{u}^{*(i)}(\mathbf{y}) \approx \mathbf{N}_u^{(i)}(\mathbf{y})\mathbf{d}_u^{(i)}, \quad \forall \mathbf{y} \in \Omega^{(i)}. \tag{19}$$

Consequently, the field of fluctuating strains $\boldsymbol{\epsilon}^*(\mathbf{y})$ is related to the nodal displacements via the geometric matrix $\mathbf{B}_u^{(i)}(\mathbf{y})$:

$$\boldsymbol{\epsilon}^{*(i)}(\mathbf{y}) \approx \mathbf{B}_u^{(i)}(\mathbf{y})\mathbf{d}_u^{(i)}, \quad \forall \mathbf{y} \in \Omega^{(i)}. \tag{20}$$

The approximation of the surface tractions $\boldsymbol{\lambda}^{[1]}(\mathbf{y})$ is performed in the analogous way:

$$\boldsymbol{\lambda}^{[1]}(\mathbf{y}) \approx \mathbf{N}_\lambda^{[1]}(\mathbf{y})\mathbf{d}_\lambda^{[1]}, \quad \forall \mathbf{y} \in \Gamma^{[1]}. \tag{21}$$

Altogether, the approximate value of the functional receives the following form:

$$\begin{aligned}\tilde{\Theta}(\mathbf{d}_u, \mathbf{d}_\lambda^{[1]}) &= \frac{1}{2}\sum_{i=1}^{n}\int_{\Omega^{(i)}}\left(2\mathbf{E}^{\mathrm{T}}\mathbf{L}^{(i)}\mathbf{B}_u^{(i)}(\mathbf{y})\mathbf{d}_u^{(i)} + \mathbf{d}_u^{(i)^{\mathrm{T}}}\mathbf{B}_u^{(i)}(\mathbf{y})^{\mathrm{T}}\mathbf{L}^{(i)}\mathbf{B}_u^{(i)}(\mathbf{y})\mathbf{d}_u^{(i)}\right)\mathrm{d}\Omega \\ &+ \sum_{j=2}^{n}\int_{\Gamma^{[j]}}\mathbf{d}_\lambda^{[1]^{\mathrm{T}}}\mathbf{N}_\lambda^{[1]}(\mathbf{y})^{\mathrm{T}}\left(\mathbf{N}_u^{(j)}(\mathbf{y})\mathbf{d}_u^{(j)} - \mathbf{N}_u^{(1)}(\mathbf{y})\mathbf{d}_u^{(1)}\right)\mathrm{d}\Gamma. \qquad (22)\end{aligned}$$

3.3 Minimization problem

Since the matrices $\mathbf{B}_u^{(i)}(\mathbf{y})^{\mathrm{T}}\mathbf{L}^{(i)}\mathbf{B}_u^{(i)}(\mathbf{y})$ are positive, the global minimum of the function $\tilde{\Theta}$ coincides with the stationary point defined by optimality conditions

$$\frac{\partial\tilde{\Theta}}{\partial\mathbf{d}_u^{(i)}} = \mathbf{0} \quad\Leftrightarrow\quad \mathbf{K}^{(i)}\mathbf{d}_u^{(i)} = \mathbf{f}^{(i)} - \boldsymbol{\mathcal{E}}^{(i)^{\mathrm{T}}}\mathbf{d}_\lambda^{[1]}, \qquad (23)$$

$$\frac{\partial\tilde{\Theta}}{\partial\mathbf{d}_\lambda^{[1]}} = \mathbf{0} \quad\Leftrightarrow\quad \sum_{i=1}^{n}\boldsymbol{\mathcal{E}}^{(i)}\mathbf{d}_u^{(i)} = \mathbf{0}. \qquad (24)$$

In the conditions (23–24), we have employed the following substitutions:

$$\mathbf{K}^{(i)} = \int_{\Omega^{(i)}}\mathbf{B}_u^{(i)}(\mathbf{y})^{\mathrm{T}}\mathbf{L}^{(i)}\mathbf{B}_u^{(i)}(\mathbf{y})\,\mathrm{d}\Omega, \qquad (25)$$

$$\mathbf{f}^{(i)} = -\int_{\Omega^{(i)}}\mathbf{E}^{\mathrm{T}}\mathbf{L}^{(i)}\mathbf{B}_u^{(i)}(\mathbf{y})\,\mathrm{d}\Omega, \qquad (26)$$

$$\boldsymbol{\mathcal{E}}^{(1)} = -\sum_{j=2}^{n}\int_{\Gamma^{[j]}}\mathbf{N}_\lambda^{[1]}(\mathbf{y})^{\mathrm{T}}\mathbf{N}_u^{(1)}(\mathbf{y})\,\mathrm{d}\Gamma, \qquad (27)$$

$$\boldsymbol{\mathcal{E}}^{(j)} = \int_{\Gamma^{[j]}}\mathbf{N}_\lambda^{[1]}(\mathbf{y})^{\mathrm{T}}\mathbf{N}_u^{(j)}(\mathbf{y})\,\mathrm{d}\Gamma. \qquad (28)$$

Following the analogy with the Finite Element treatment of dynamics of structures, e.g. (Bittnar and Šejnoha, 1996), the matrices $\boldsymbol{\mathcal{E}}^{(i)}$ defined by (27) and (28) will be called *consistent*, while the Boolean matrices (sparse matrices containing only ones and zeros) are referred to as *lumped* ones. The latter option is used in the actual implementation, which corresponds to enforcing the displacement compatibility conditions at individual nodes of the finite element mesh.

3.4 Dual formulation

Now we proceed with expressing the coefficients of fluctuating displacements $\mathbf{d}_u^{(i)}$ from the systems of equations (23) in the form

$$\mathbf{d}_u^{(i)} = \mathbf{K}^{(i)^\dagger}\left(\mathbf{f}^{(i)} - \boldsymbol{\mathcal{E}}^{(i)^{\mathrm{T}}}\mathbf{d}_\lambda^{[1]}\right) + \mathbf{R}^{(i)}\mathbf{d}_R^{(i)}. \qquad (29)$$

The first term $\mathbf{K}^{(i)^\dagger}\left(\mathbf{f}^{(i)} - \boldsymbol{\mathcal{E}}^{(i)^{\mathrm{T}}}\mathbf{d}_\lambda^{[1]}\right)$ in relation (29) corresponds to the particular solution of the i-th component of the system (23), which is expressed by the help of the generalized inverse matrix $\mathbf{K}^{(i)^\dagger}$ (see Gruber (2007) or Kruis (2006) for further discussion), replacing the inverse

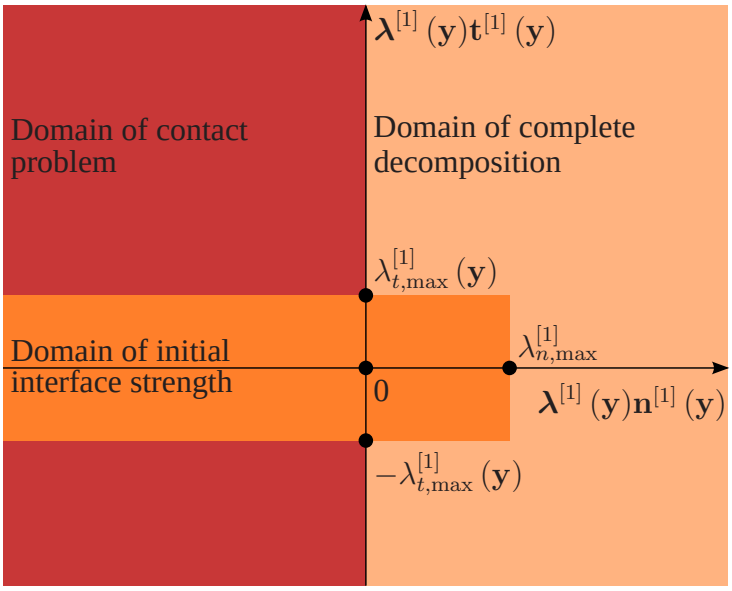

Figure 2: Graphical interpretation of constitutive law on interface.

matrix for singular $\mathbf{K}^{(i)}$. The second term $\mathbf{R}^{(i)}\mathbf{d}_R^{(i)}$ appearing in Equation (29) corresponds to a homogeneous solution of the system of the i-th component of the system (23), expressed as the linear combination of rigid body motions $\mathbf{R}^{(i)}$ with coefficients of the linear combination $\mathbf{d}_R^{(i)}$. Next, we substitute the coefficients of fluctuating displacements $\mathbf{d}_u^{(i)}$ from relations (29) to system (24) and add the solvability conditions (31) to account again for a possible singularity of matrices $\mathbf{K}^{(i)}$:

$$\sum_{i=1}^{n} \boldsymbol{\mathcal{E}}^{(i)}\mathbf{K}^{(i)\dagger}\boldsymbol{\mathcal{E}}^{(i)\mathrm{T}}\mathbf{d}_\lambda^{[1]} - \sum_{i=1}^{n} \boldsymbol{\mathcal{E}}^{(i)}\mathbf{R}^{(i)}\mathbf{d}_R^{(i)} = \sum_{i=1}^{n} \boldsymbol{\mathcal{E}}^{(i)}\mathbf{K}^{(i)\dagger}\mathbf{f}^{(i)} \tag{30}$$

$$\mathbf{R}^{(i)\mathrm{T}}\left(\mathbf{f}^{(i)} - \boldsymbol{\mathcal{E}}^{(i)\mathrm{T}}\mathbf{d}_\lambda^{[1]}\right) = \mathbf{0} \tag{31}$$

Elimination of the primary unknowns $\mathbf{d}_u^{(i)}$ in (23–24) leads to a dual problem, formulated in terms of $\mathbf{d}_\lambda^{[1]}$ and $\mathbf{d}_R^{(i)}$. This problem can be efficiently solved using the Modified Conjugate Gradient (MCG) method, augmented by the projection step to ensure the solvability condition (31), see again (Kruis, 2006) or (Gruber, 2007) for further details.

3.5 Constitutive law on interface

As the final ingredient of the problem formulation, the particular form of the constitutive law is shown in Figure 2. In the framework of the proposed FETI-based algorithm, such a constitutive assumption leads to the following conceptual implementation of the debonding problem:

INPUT 1: properties of individual constituents, initial conditions on interface
INPUT 2: normal $\lambda^{[1]}_{n,\max}(\mathbf{y})$ and tangential $\lambda^{[1]}_{t,\max}(\mathbf{y})$ strength of interface
INPUT 3: final macroscopic load (macro-strain $\mathbf{E}$)
INPUT 4: $N =$ number of load steps

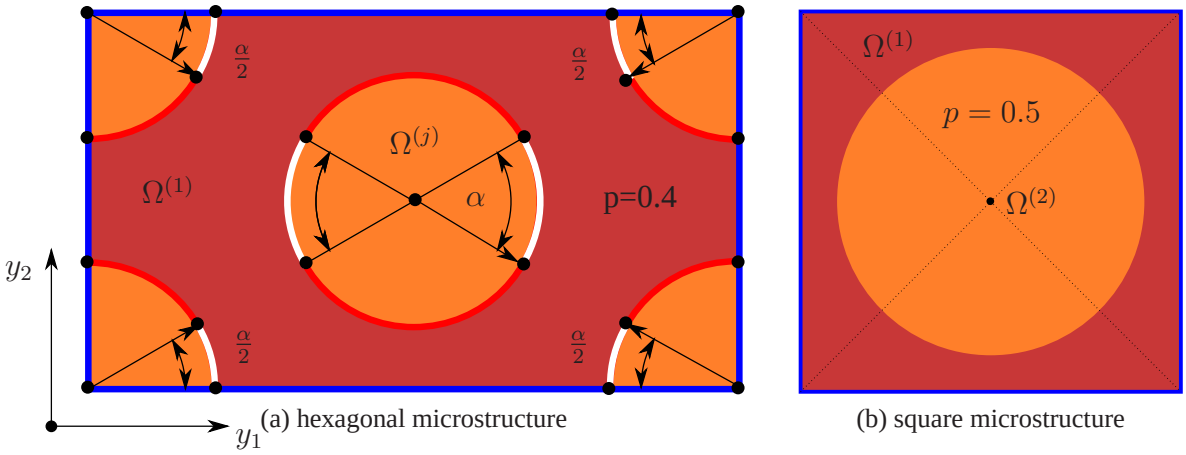

(a) hexagonal microstructure (b) square microstructure

Figure 3: PUCs used in numerical experiments.

LOOP 1: for $i = 1$ to N
Apply macrostrain $i/N \cdot \mathbf{E}$ to a PUC
LOOP 2: repeat until the interfacial conditions are unchanged
MCG $\Rightarrow$ evaluate actual values of normal and tangential surface tractions
SWITCH (in terms of actual values of surface tractions)
1. Domain of initial interface strength (Figure 2)
$\Rightarrow$ surface tractions are unchanged
2. Domain of contact problem (Figure 2)
$\Rightarrow$ surface tractions in tangential direction set to zero (irreversible)
3. Domain of complete decomposition (Figure 2)
$\Rightarrow$ surface tractions in both direction set to zero (irreversible)
END SWITCH
END LOOP 2
computation of actual primal unknowns – evaluation of displacements inside the domains $\Rightarrow \boldsymbol{\Sigma}$
END LOOP 1

Note again that, due to the adopted lumped form of the "continuity" matrices $\boldsymbol{\mathcal{E}}^{(i)}$, the constitutive law is applied in discretized form, i.e. the value of surface tractions is converted to equivalent nodal forces.

4 Numerical examples

In this section we show results of selected numerical experiments obtained using an in-house code implemented in MATLAB 7.1. All reported examples were executed on one of the PUCs appearing in Figure 3.

4.1 Controlled perfect debonding of constituents

In this experiment, we compare the macroscopic stress $\boldsymbol{\Sigma}$ computed using the FETI method with the results available in (Šejnoha and Srinivas, 1998), corresponding to the hexagonal mi-

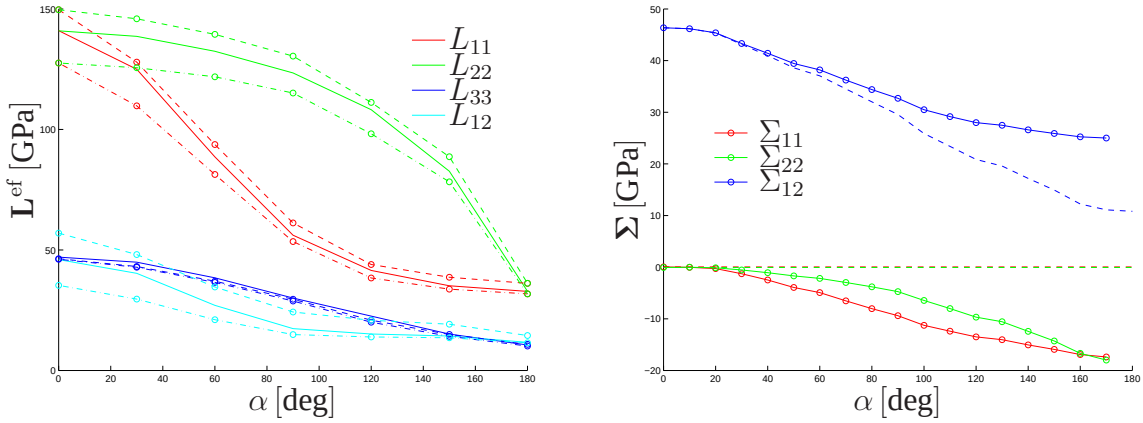

(a) with penetration

(b) without penetration

Figure 4: Dependence on the overall response on the debonding angle α.

crostructure represented by a PUC shown in Figure 3a. Both the plane stress and the plane strain assumptions were used in the analysis to provide a comparison with a three-dimensional simulations (Šejnoha and Srinivas, 1998). The PUC cell with 40% of fibers ($p = 0.4$) and material data

$$\begin{array}{rcl} E_y^{(1)} & = & 88\,\mathrm{GPa} \\ \nu^{(1)} & = & 0.299 \end{array} \quad \text{and} \quad \begin{array}{rcl} E_y^{(2)} & = & 200\,\mathrm{GPa} \\ \nu^{(2)} & = & 0.299 \end{array}, \tag{32}$$

were used. Note that $E_y^{(i)}$ and $\nu^{(i)}$ denote the Young modulus and the Poisson ratio of the i-phase, respectively. The PUC was loaded by three elementary load cases

$$\mathbf{E} = [1,0,0]^{\mathrm{T}}, \quad \mathbf{E} = [0,1,0]^{\mathrm{T}}, \quad \mathbf{E} = [0,0,1]^{\mathrm{T}}, \tag{33}$$

and the corresponding macroscopic stress $\boldsymbol{\Sigma}$ was computed to arrive at the effective stiffness matrix $\mathbf{L}^{\mathrm{ef}}$. The resulting dependence of the effective stiffness matrix on the debonding angle α appears in Figure 4a. The dashed line and the dot-and-dashed line display the results computed for the plane strain and the plane stress, respectively. The continuous line represents the results from (Šejnoha and Srinivas, 1998) (i.e. the three-dimensional PUC). Note that all data correspond to the case *without* contact conditions, i.e. the individual constituents can overlap freely. Evidently, very good match between reference results and the FETI-base procedure has been achieved. Moreover, it can be seen that the plane strain response provides an upper bound to the three-dimensional response, while the plane stress conditions result in a lower bound.

To further illustrate the influence of the contact condition between the individual constituents, the PUC was loaded by the shear macroscopic strain

$$\mathbf{E} = [0,0,0.2]^{\mathrm{T}}. \tag{34}$$

The deformed shapes of the PUCs are compared in Figure 5; Figure 4b offers additional quantitative comparison between these two cases. The dashed and continuous lines in Figure 4b denote the results without and with activation of the contact, respectively. The FETI-based algorithm correctly prevents the interpenetration of individual phases, see Figure 4b, which leads to a slightly more stiff shear response and to the appearance of an additional normal stress when compared with the former approach.

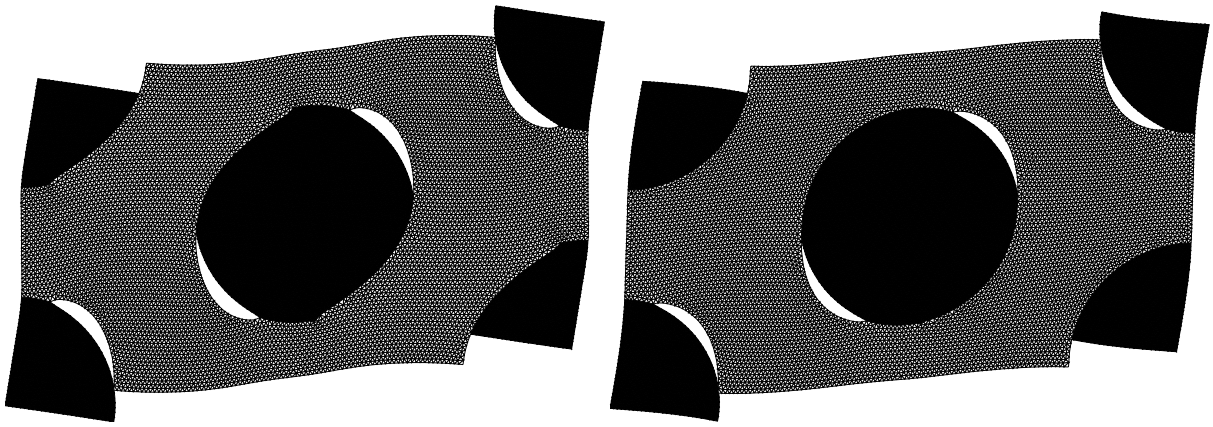

(a) with penetration (b) without penetration

Figure 5: Overall deformation of PUC.

4.2 Load induced complete debonding of constituents

Finally, Figure 6 plots the macroscopic stress-strain curves, determined for the composite shown in Figure 3b in the plane stress state, subject to the macroscopic deformation

$$\mathbf{E} = [0.2, 0, 0]^{\mathrm{T}}. \tag{35}$$

and the following material data are used in the simulation

$$\begin{array}{rcl} E_y{}^{(1)} & = & 100\,\mathrm{GPa} \\ \nu^{(1)} & = & 0.4 \end{array} \quad \text{and} \quad \begin{array}{rcl} E_y{}^{(2)} & = & 500\,\mathrm{GPa} \\ \nu^{(2)} & = & 0.2. \end{array} \tag{36}$$

The continuous line and dotted lines, appearing in Figure 6, display the normal macroscopic stress $\boldsymbol{\Sigma}$ in the direction of the nonzero macroscopic deformation $\mathbf{E}$ and orthogonal direction of the nonzero macroscopic deformation $\mathbf{E}$, respectively. Recall that in Figure 6, $\lambda^{[1]}_{n,\max}$ and $\lambda^{[1]}_{t,\max}$ denote the normal and the tangential strength whole interface, respectively; the symbol j stands for a unit of length. It can be seen that the proposed numerical method is able to capture the complex interaction between the debonding and the inter-phase contact; a mechanism which is notoriously difficult to capture by existing analytical approaches of the continuum micromechanics.

5 Conclusions

In the current work, a brief overview of a FETI-based procedure for the homogenization of composite materials developed in (Gruber, 2007) has been presented. The most important conclusions can be summarized as follows:

- The proposed numerical scheme is very efficient in handling the problems, which are difficult to be treated by the displacement-based FEM approaches such as the non-penetration of individual phases and traction-based interfacial constitutive laws.
- The method is fully capable of capturing complex non-linear response typical of heterogeneous materials.

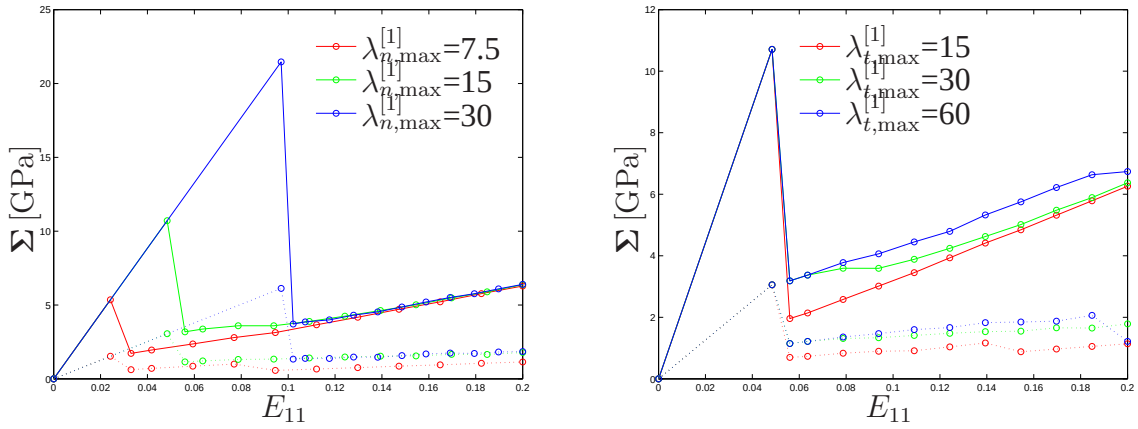

(a) $\lambda^{[1]}_{t,\max}$=30 (b) $\lambda^{[1]}_{n,\max}$=15

Figure 6: Effective stress-strain diagrams. Initial interface strength in $\mathrm{GN/j}$.

In the current state, the method is limited to specific, quite simplistic, constitutive laws for the interfacial region. Moreover, to fully assess the added value of the duality-based approach, more extensive comparison with the existing micro-mechanical methods should be performed. These topics are currently under investigation and will be reported separately.

Acknowledgments

Financial support of this work provided by the Grant Agency of the Czech Republic, projects GAČR 106/08/1379 and GAČR 106/07/1244, is gratefully acknowledged.

References

Areias, P. M. A. and Rabczuk, T. (2008). Quasi-static crack propagation in plane and plate structures using set-valued traction-separation laws. *International Journal for Numerical Methods in Engineering*, 74(3):475–505.

Bittnar, Z. and Šejnoha, J. (1996). *Numerical methods in structural mechanics*. ASCE Press and Thomas Telford, Ltd, New York and London.

Cox, B. and Yang, Q. (2006). In quest of virtual tests for structural composites. *Science*, 314(5802):1102–1107.

Dostál, Z., Horák, D., and Vlach, O. (2007). Feti-based algorithms for modelling of fibrous composite materials with debonding. *Mathematics and Computers in Simulation*, 76(1-3):57–64.

Farhat, C. and Roux, F.-X. (1991). A method of finite element tearing and interconnecting and its parallel solution algorithm. *International Journal for Numerical Methods in Engineering*, 32(6):1205–1227.

Gruber, P. (2007). Homogenization of composite materials with imperfect bonding of constituents. Master's thesis, Czech Technical University, Prague. (in Czech), http://mech.fsv.cvut.cz/~grubepav/download/gruber_master_thesis.pdf.

Kruis, J. (2006). *Domain Decomposition Methods for Distributed Computing*. Saxe-Coburg Publications, Kippen, Stirling, Scotland, druh edition.

Kruis, J. and Bittnar, Z. (2008). Reinforcement-matrix interaction modeled by feti method. In *Domain Decomposition Methods in Science and Engineering XVII*, pages 567–573. Springer Verlag.

Li, S. and Ghosh, S. (2004). Debonding in composite microstructures with morphological variations. *International Journal of Computational Methods*, 1(1):121–149.

Matouš, K., Inglis, H. M., Gu, X., Rypl, D., Jackson, T. L., and Geubelle, P. H. (2007). Multiscale modeling of solid propellants: From particle packing to failure. *Composites Science and Technology*, 67(7–8):1694–1708.

Michel, J. C., Moulinec, H., and Suquet, P. (1999). Effective properties of composite materials with periodic microstructure: a computational approach. *Computer Methods in Applied Mechanics and Engineering*, 172(1-4):109–143.

Rektorys, K. (2007). *Variational Methods in Mathematics, Science and Engineering*. Springer Verlag, second edition.

Somolová, A. (2007). Homogenization applied to civil engineering structures. Master's thesis, Czech Technical University, Prague. (in Czech), http://mech.fsv.cvut.cz/~zemanj/teaching/theses/somolova_07.pdf.

Šejnoha, M. and Srinivas, M. (1998). Modeling of effective properties of composites with interfacial microcracks using PHA model. *Building Research Journal*, 46(2):99–108.

Wikipedia (2007). Voigt notation — Wikipedia, The free encyclopedia. [Online; accessed 17-December-2007].